Design of a photonic crystal microcavity for biosensing*

Li Junhua(李俊华)[†], Kan Qiang(阚强), Wang Chunxia(王春霞), Su Baoqing(苏保青),
Xie Yiyang(解意洋), and Chen Hongda(陈弘达)

State Key Laboratory Integrated Optoelectronics, Institute of Semiconductors, Chinese Academy of Sciences,
Beijing 100083, China

Abstract: We have designed an air-bridged PhC microcavity with high sensitivity and a high quality factor. The structure parameters of the microcavity are optimized by three-dimensional finite-difference time-domain method. We compare the performance of a silicon-on-insulator PhC microcavity and an air-bridged PhC microcavity, and analyze the effect of the thickness of the slab and the radius of the defect hole on the performance of the air-bridged PhC microcavity. For a thinner slab and a larger defect hole, the sensitivity is higher while the quality factor is lower. For the air-bridged photonic crystal slab, the sensitivity can reach 320-nm/RIU (refractive index unit) while the quality factor keeps a relatively high value of 120 by selecting the proper slab thickness and the defect hole radius, respectively, when the refractive index is 1.33. This is meaningful for low-detection-limit biosensing.

Key words: air-bridged PhC microcavity; biosensing; sensitivity; quality factor; defect mode

1. Introduction

Label-free affinity-based optical biosensors have been pursued with great interest over the past few years[1−6], because they do not require the use of radioactive/fluorescent labels that introduce complexity and potential contamination to biological material in vivo. Generally, affinity-based sensors detect the selective binding between target molecules and capture agents. They not only simplify sample preparation by avoiding staining but also allow researchers to record processes such as protein recognition in real time. The well-developed label-free platforms include surface plasmon resonance (SPR)[1], microrings[5, 6], waveguides[7], and one dimensional photonic bandgap structures, ranging from simple Bragg reflectors[8] to microcavities[9] built with porous silicon. Photonic crystals (PCs) are an attractive sensing platform because they provide strong light confinement. Unlike many other sensing platforms that utilize the interaction between the small evanescent tail of the electromagnetic field and the analyte, PCs can be designed to localize the electric field in the low refractive index region (e.g. air pores), which makes the sensors extremely sensitive to a small refractive index change produced by bio-molecule immobilization on the pore walls[10].

Recently, 2-D photonic crystal (PhC) microcavities, formed by introducing a defect in an otherwise perfectly periodic structure, have shown great promise for chemical[11] and biological[12] sensing because of the high electric field concentration in the small modal volume of PhC microcavities, which leads to efficient light–matter interaction with minuscule volumes (∼ 1 fL) of analyte[3]. Such ultra-small devices are crucial for biochemical sensors because the amount of sample is often limited. Moreover, the miniaturization of the sensing devices makes very compact photonic integrated chips possible.

In this paper, we focus on the design and optimization of the PhC cavity to achieve higher resolution and larger sensitivity for index sensing by increasing the overlapping of electric field with the background material. The optimizations are performed in three ways, including thinning slab thickness, varying the radius of the central defect hole and using an air-bridged structure.

Two parameters are quite important for the performance of sensors. One is sensitivity (S) and another is the quality factor (Q). S is defined as $S = \frac{\Delta \lambda}{\Delta n}$, where $\Delta \lambda$ is the change in the resonant wavelength and Δn is the change in the background refractive index. Q is defined as $\frac{\omega_0 U(t)}{P(t)}$, where ω_0 is the angular resonant frequency, $U(t)$ is the energy stored in the cavity mode, and $P(t)$ is the energy dissipated per cycle. By tuning the structure parameters, we theoretically investigate S and Q for the microcavitity to optimize our device design through three-dimensional (3D) finite-difference time-domain (FDTD) simulations using a commercial FDTD software package (FDTD Solutions–Lumerical). For the optimized air-bridge photonic crystal slab, the microcavity sensitivity can reach 320 nm/RIU by selecting proper slab thickness and the defect hole radius, respectively.

2. Design of the PhC microcavity

The photonic crystal structure in this paper consists of a triangular array of cylindrical air holes with a lattice constant a = 440 nm. The photonic crystal is designed with a hole radius r = 127.5 nm = 0.29a. The microcavities analyzed in this paper are formed by introducing a point defect into the PhC. A simple method of forming a microcavity within the structure is to change the radius of the central hole, as shown in the schematic structure in Fig. 1(a). By increasing the radius of the
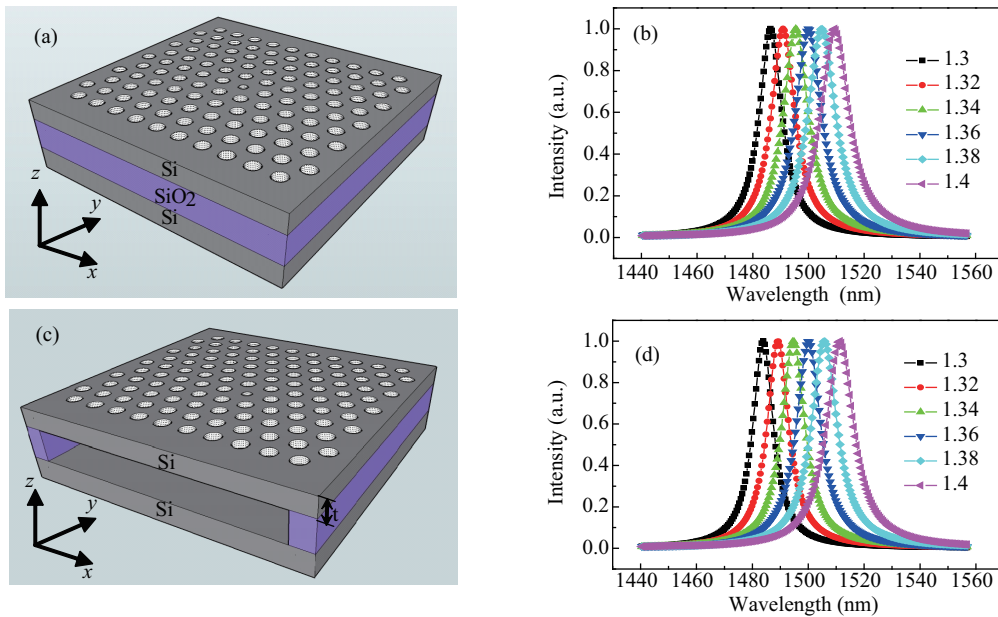
Fig. 1. (a) Photonic crystal microcavity designed on silicon-on-insulator materials. The grey area indicates Si and the purple area indicates SiO$_2$. (b) Normalized transmission spectra corresponding to Fig. 1(a) with six different background refractive indices ranging from $n = 1.3$ to $n = 1.4$ in 0.02 increments. (c) Photonic crystal microcavity designed on an air-bridged silicon slab. (d) Normalized transmission spectra corresponding to Fig. 1(c) with six different background refractive indices ranging from $n = 1.3$ to $n = 1.4$ in 0.02 increments.

central hole, an acceptor defect state pulled from the dielectric band into the band-gap is excited[13], while by decreasing the radius of the center hole a donor defect state is pulled into the band-gap from the air band. Acceptors tend to concentrate their electric field energy density in regions where the larger refractive index is located in the unperturbed PhC, while the electric field energy density of donors is to the contrary. Since the electric field intensity in air regions is small in case of acceptor defects, they are not good candidates for monitoring the refractive index (RI) change in the background material. So in this article we will focus on the donor states excited by decreasing the radius of the central hole.

Here, we have simulated two different structures. One is a silicon-on-insulator (SOI) photonic crystal slab (Fig. 1(a)) structure which was experimentally studied by Chow *et al.*[3] and Lee *et al.*[12] recently, and another is an air-bridged photonic crystal slab structure (Fig. 1(c)), which provides a better performance for sensing applications than the former. The biosensing principle for the two structures is the same. The defect hole of the PhC disturbs the PhC's period structure, leading to the formation of the defect mode in the band gap. Light resonates with the defect mode can propagate in the PhC. As a result, the defect mode appears as a sharp peak within the band gap on the transmission (or reflection) spectrum. The high electric field concentration results from Bragg reflection in the in-plane directions and total internal reflection(TIR) in the vertical direction makes the defect mode position highly sensitive to changes in the refractive index of the surrounding medium. The structures in our simulation contain four layers of air holes on each side of the defect in the plane of the PhC slab. Considering that there is no band gap for the TM mode if the RI contrast and r/a is not large enough[14], we use magnetic dipole sources with magnetic field polarized along the z direction to activate the TE-like mode in the microcavity. In addition, we

use symmetry boundary conditions along the x and z directions and antisymmetry boundary conditions along the y direction to achieve an eight-fold reduction in the computational grid size. In the central region of the microcavity, the smallest grid spacing used corresponds to $a/16 = 27.5$ nm along the x and y directions.

For the SOI structure, the top Si slab with thickness $t = 0.591a$ is separated from the Si substrate by 1 μm SiO$_2$, and for the air-bridged structure, the Si slab thickness is also $0.591a$. The central defect hole radius $r_d = 0.2a$ for both structures. The sensing area is located at the center hole in the 10 μm^2 scale. Figures 1(b) and 1(d) are the normalized transmission spectra with a background refractive index ranging from $n = 1.3$ to $n = 1.4$ in 0.02 increments. With the increase in refractive index, the resonated mode position forms a linear red-shift, as can be seen from Fig. 2(a). For the SOI PhC microcavity, S is 230 nm/RIU (refractive index unit) while for the air-bridged PhC microcavity S is 275-nm/RIU. What's more, Figure 2(b) shows that the air-bridged PhC microcavity possesses a relatively higher quality factor than the SOI PhC microcavity. Considering these two factors, the air-bridged PhC microcavity is a better candidate for biosensing. Thus, in the following section, we will focus on optimizing the sensing performance of the air-bridged structure by optimizing the defect hole radius and the slab thickness

.

3. Effect of slab thickness on S and Q in the air-bridged PhC microcavity

Slab thickness is a key parameter for the performance of a microcavity. The related parameters in Fig. 3 are $a = 440$ nm, $r_d = 0.2a$ and $r = 0.29a$. Figure 3(a) shows that with increasing background material refractive index, the resonant wavelength
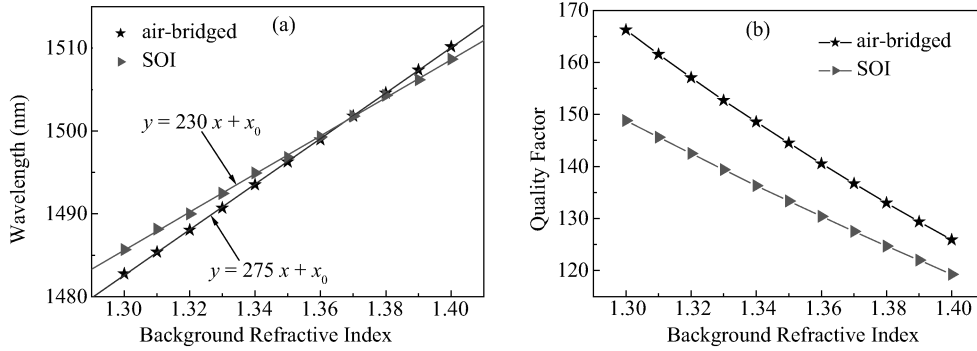
Fig. 2. (a) Resonant wavelength versus background index. (b) Quality factor versus background refractive index.
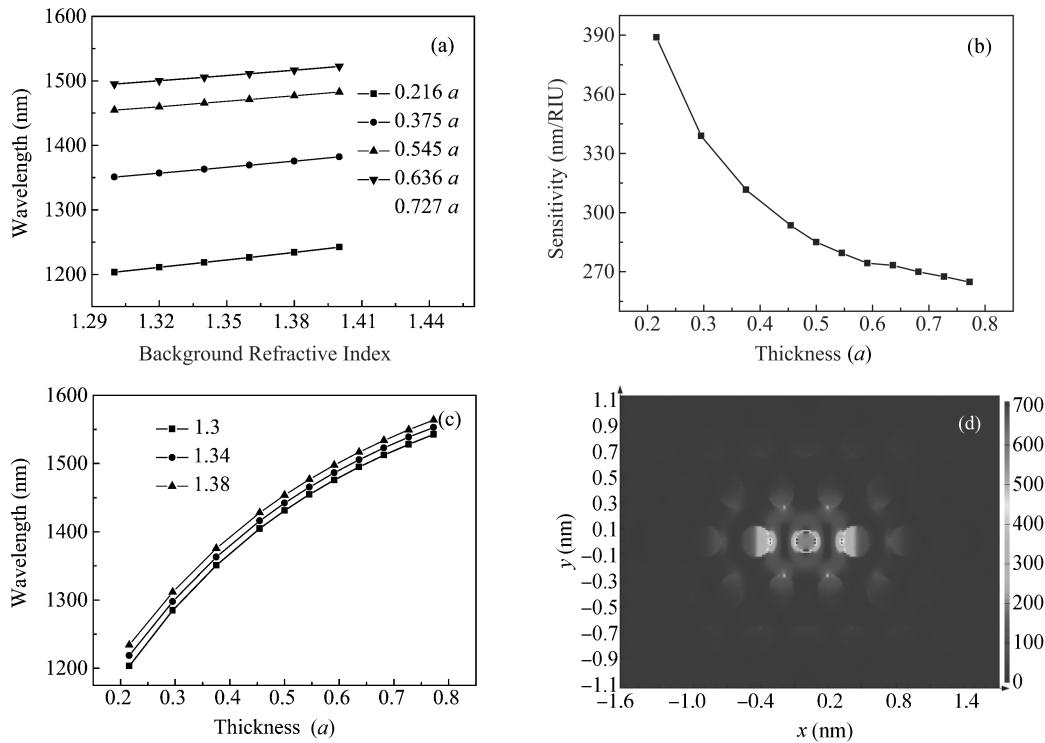

Fig. 3. (a) Calculated resonant wavelength plotted vs background material refractive index for different slab thicknesses indicated in the legend. (b) Sensitivity as a function of the slab thickness, which is indicated in units of lattice constant a. (c) Resonant wavelength plotted versus. slab thickness for different background RI shown in the legend. (d) Electric field intensity pattern in the microcavity. Parameters of the structure are $r_d = 0.2a$, $r = 0.29a$, $t = 0.591a = 260$ nm, and the RI of the background material is 1.32. The plotted intensity pattern is for the $x−y$ plane at the middle of the slab.

of the microcavity increases linearly for each slab thickness indicated in the legend. This is because the increase in the background RI will reduce the RI contrast between the Si slab and the background material, which will make the frequency of the donor mode move towards the lower edge of the bandgap[14], resulting in a redshift of the resonant wavelength. What's more, the reduction in the RI contrast will make the confinement of the electric field weaker, so more electric field will be distributed outside the slab, inducing a lower quality factor, which can be seen in Fig. 4(d). In order to minimize the losses into the substrate, the index contrast between the slab and the background material should be as large as possible.

The slab thickness is important for S and Q for two reasons. First, it seriously affects the field distribution. Figure 4(b) is the electric field distribution for $t = 260$ nm $= 0.591a$,

from which we can see that the defect mode is mostly confined inside the slab and the evanescent field of the mode experiences the background material. In the electric field intensity distribution along the z-axis shown in Fig. 4(b), a very small portion of the electric field is distributed in the background. The mode size can be characterized by the full-width half-maximums (FWHM) of the field distribution along the z-axis[15]. For Fig. 4(c), we calculate that the FWHM is $0.59a$, i.e. 260 nm, just the thickness of the slab, which means that at the edge of the slab, the electric intensity has just attenuated to half of the maximum. Figure 4(e) is the electric field distribution for $t = 0.216a$. It's easy to find that the larger fraction of the mode energy is distributed in the background material. The mode size along the z-axis becomes smaller and the FWHM is $0.426a$, i.e. 187.7 nm. For a thinner slab, the
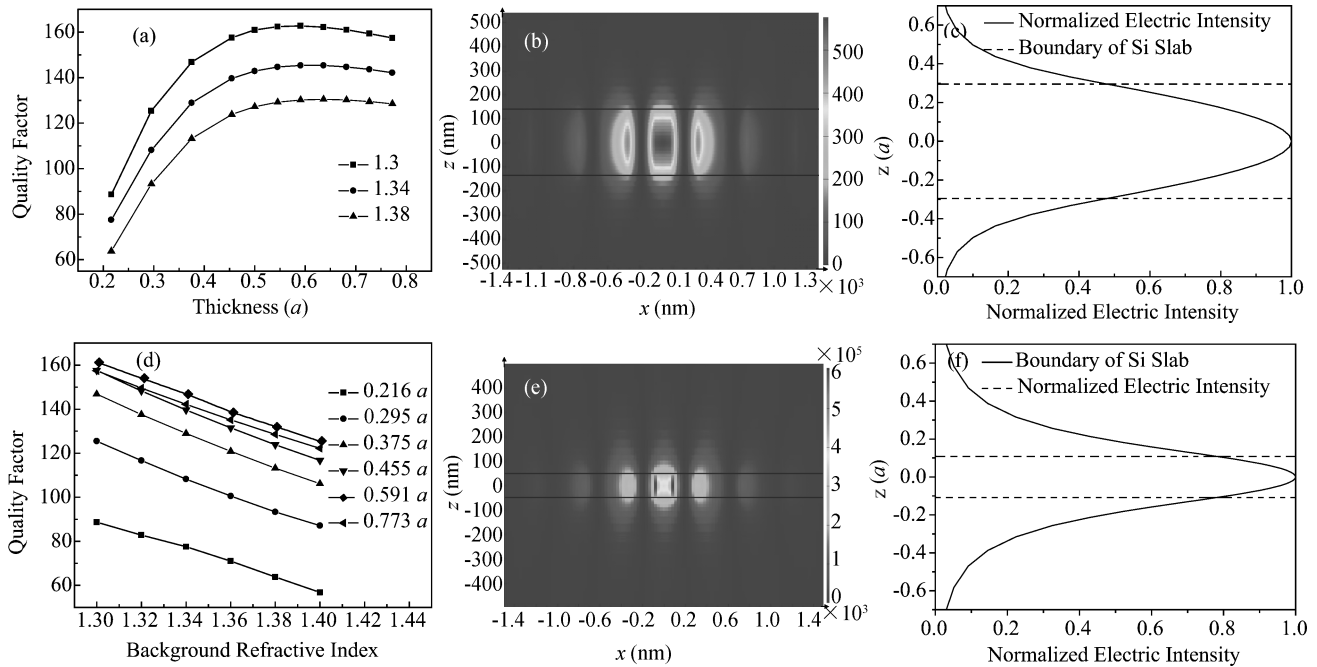
Fig. 4. (a) Quality factor as a function of Si slab thickness with different background refractive indices shown in the legend. (b) Electric intensity profile in the $x-z$ plane through the center of the defect hole for slab thickness $t = 260$ nm $= 0.591a$. The black solid lines indicate the boundaries of the Si slab. Parameters of the structures are $r_d = 0.2a$, $r = 0.29a$, and the RI of the background material is 1.32. (c) Normalized Electric intensity distribution along the z-axis for Fig. 4(b). (d) Quality factor as a function of background refractive index with the thickness indicated in the legend. (e) Electric intensity profile in the $x-z$ plane through the center of the defect hole for slab thickness $t = 95$ nm $= 0.216a$. The black solid lines indicate the boundaries of the Si slab. The other parameters are the same as those described in Fig. 4(b). (f) Normalized Electric intensity distribution along the z-axis for Fig. 4(e).

evanescent field component is larger and the mode size in the cavity is smaller. These effects strongly affect S and Q. The larger overlap of the field distribution with the background material and the larger the mode size, the smaller the quality factor and the larger the sensitivity. Our simulations have verified this argument. Figure 3(b) indicates that a thinner Si slab has higher sensitivity. For slab thickness $t = 0.216a$, the sensitivity is 388.9-nm/RIU, while for $t = 0.773a$, it decreases to 264.8 nm/RIU. The descending trend is monotone as the slab thickness increases, but it slows down as the thickness increases. Figure 4(a) shows that Q increases as the thickness increases. Whereas when the thickness reaches $0.5a$, Q becomes saturated. S also varies slowly when the thickness is larger than $0.5a$. So $0.5a$ is large enough to confine most of the energy to the microcavity. From Fig. 4(c), we can see that most of the electric intensity is distributed in the defect hole, so the index change in the defect hole makes the greatest contribution to the sensing response. To verify this point, we perform a simulation in which the background material index varies apart from the area in the slab. For $r_d = 0.2a$, $r = 0.29a$ and $t = 0.591a$, we find that the sensitivity is just 40 nm/RIU, in contrast with a much higher sensitivity of 274.3 nm/RIU if the RI of all the background material changes, which is inconsistent with this point. Second, the thickness of the slab will affect the energy band. As the thickness decreases, the edge of the slab material (Si) band and the background material will increase, owing to increasing photon momentum in the z direction[14]. A simple explanation could be made using the uncertainty principle in quantum mechanics. The uncertainty principle for the case above can be expressed as $tp_z = h$, where t is the thick-

ness of the slab, p_z is the momentum normal to the slab, and h is the Planck constant. As t decreases, p_z will increase while the momentum parallel to the slab stays invariant. So the total momentum will increase, corresponding to the increase in the resonant frequency of the defect modes. Thus, the resonant wavelength will increase with the increase in the slab thickness, as shown in Fig. 3(c). As the PhC microcavity with a thinner slab has a larger S and smaller Q, a trade-off between S and Q is necessary. From Figs. 4(a) and 3(b), we find that when $t = 0.375a$, Q is 147 and S is 311.6 nm/RIU for RI = 1.3. Both parameters are relatively satisfactory, so $t = 0.375a$ is our choice.

4. Effect of defect radius on S and Q in the air-bridged PhC microcavity

The radius of the defect hole is another important parameter for S and Q. As we know, for a perfect PhC, there is no mode in the band gap. By decreasing the radius of a single hole (defect hole), a donor mode is excited and the smaller the defect hole, the lower the donor mode frequency in the bandgap. Thus, increasing the defect hole radius will give rise to a blue-shift of the resonant wavelength, as illustrated in Fig. 5(a). The donor mode tends to concentrate electric field energy in the regions of the PhC where a lower refractive index is located[16], which means that more energy is distributed in the defect hole. This is the case in Fig. 4(d). With the increase in the defect hole radius, the overlapping of the field with the background material will become greater, resulting in a larger sensitivity, as shown in Fig. 5(b). When the defect hole is completely re-
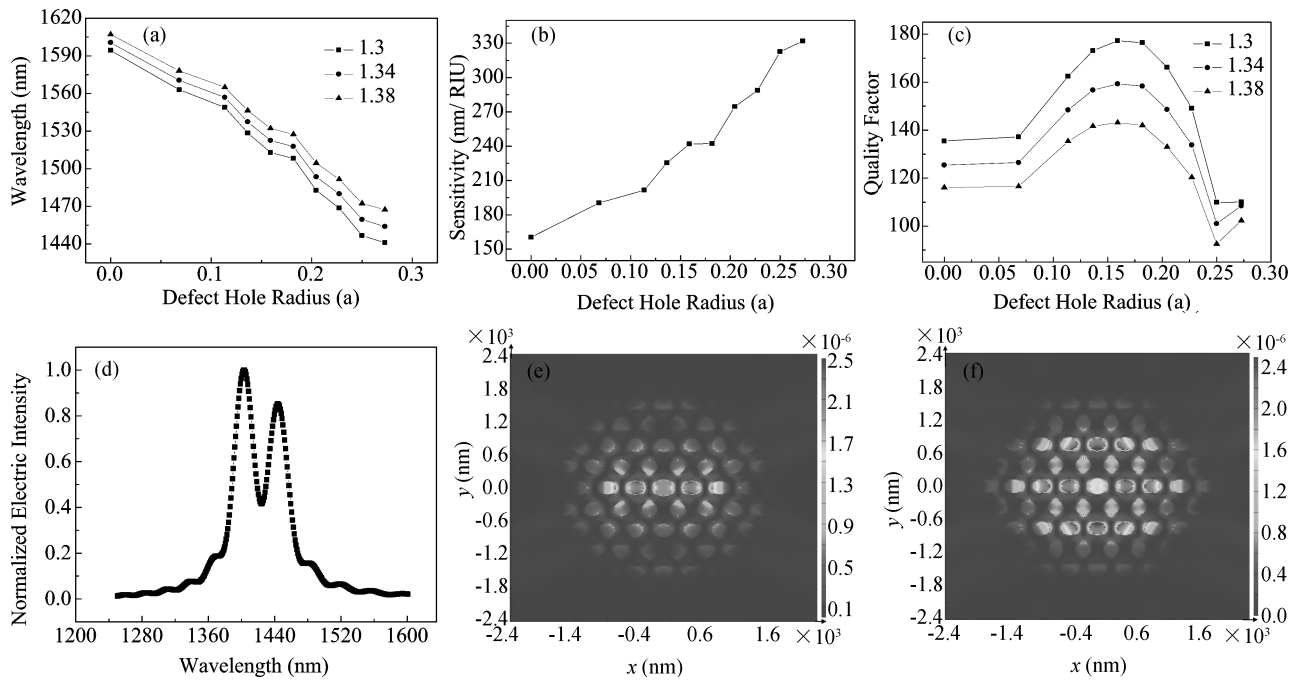
Fig. 5. (a) Resonant wavelength versus defect hole radius for the background index shown in the legend. The parameters of the structures are $r = 0.29a$ and $t = 0.591a$. (b) The sensitivity varies with the defect hole radius for $r = 0.29a$ and $t = 0.591a$. (c) The quality factor varies with the defect hole radius for the background index shown in the legend. (d) As the defect radius increases to a value larger than the PhC hole radius, two resonant peaks appear. The parameters of the related structures are $r = 127.5$ nm $= 0.29a$, $r_d = 150$ nm $= 0.341a$ and $t = 0.591a$. The RI of background is 1.32. (e) The electric intensity profile in the $x-y$ plane for the peak at 1405 nm for the structure used in Fig. 6(d). (f) The electric intensity profile in the $x-y$ plane for the peak at 1445 nm for the structure used in Fig. 6(d).

moved by filling it with the slab material Si (i.e. $r_d = 0$), the sensitivity is just 160 nm/RIU, whereas when the defect radius increases to $0.273a$ (120 nm), the sensitivity is 332 nm/RIU. Figure 5(c) shows that the quality factor increases at the beginning as the defect radius increases, but when r_d reaches $0.182a$ (80 nm), it begins to drop as r increases. Especially at $r_d = 0.205a$, the slope is very steep. This may be explained as follows. Increasing r/a in the range we concern will lead to an increase in the defect mode in the bandgap and a reduction in lateral losses[16], so Q increases at first. However, the larger r_d case has larger vertical edge-scattering, which will increase vertical losses. Moreover, for larger r_d, the corresponding defect mode in the band gap is closer to the lower edge of the band for background material because a larger r_d corresponds to a larger resonant frequency, as indicated by Fig. 5(a). So the confinement for the mode energy is weaker. As r_d reaches $0.205a$, the defect mode becomes leaky in the background material. As a result, Q drops seriously. Therefore, enlarging the defect hole guarantees higher sensitivity. However, when r_d is close to r, Q of the defect mode will drop seriously. So we have to make a trade-off between S and Q when choosing the defect hole radius. From Figs. 5(b) and 5(c), we find that when $r_d = 0.227a$, Q is 149 and S is 288.7 nm/RIU for RI = 1.3. Both parameters are relatively satisfactory, so $r_d = 0.227a$ is our choice.

In addition, when r_d is larger than r, the acceptor mode is excited and the electric intensity in the defect hole is reduced by several orders. Energy is distributed in a much larger region, as shown in Figs. 5(e) and 5(f). In this case, Q is very low even though S is relatively large. Furthermore, the previous single resonant peak now degenerates into two peaks, just as Figure 5(d) indicates, for which the defect radius is $r_d = 150$ nm $= 0.341a$.

5. Conclusion

In this paper, we have in detail calculated and analyzed the effects of slab thickness and the radius of the central defect hole on S and Q by the 3D FDTD method. First, we compared the performance of an SOI PhC microcavity and an air-bridged PhC microcavity and found that the air-bridged PhC microcavity is superior to the SOI PhC microcavity, both in sensitivity and in quality factor, so we chose the air-bridged structure for further optimization. Then, we investigated the thickness effect on S and Q. For a thinner slab, S is larger and Q is smaller because of less confinement and larger overlapping of the electric intensity with the background material. By making a trade-off, we found that $t = 0.375a$ is the best choice. Third, we varied the radius of the defect hole between zero and the value of the PhC hole. The microcavity formed by a larger central defect hole tends to have a larger S and a smaller Q due to larger overlapping and weaker horizontal confinement. However, when r_d is larger than r, Q will degrade seriously and multiple peaks close together will appear, which is not ideal for biosensing applications because of the low detection limit. We select $r_d = 0.227a$ for the trade-off of the sensitivity and the quality factor. In conclusion, we design an air-bridged PhC microcavity with $t = 0.375a$ and $r_d = 0.227a$, and calculate that the relative S and Q are 320 nm/RIU and 120 when the background refractive index is 1.33.

References

[1] Liedberg B, Lundström I, Stenberg E. Principles of biosensing with an extended coupling matrix and surface plasmon resonance. Sensors and Actuators B: Chemical, 1993, 11(3): 63

[2] Zlatanovic S, Mirkarimi L W, Sigalas M M, et al. Photonic crystal microcavity sensor for ultracompact monitoring of reaction kinetics and protein concentration. Sensors and Actuators B: Chemical, 2009, 141(1): 13

[3] Chow E, Grot A, Mirkarimi L W, et al. Ultracompact biochemical sensor built with two-dimensional photonic crystal microcavity. Opt Lett, 2004, 29(10): 1093

[4] Smith C L C, Wu D K C, Lee M W, et al. Microfluidic photonic crystal double heterostructures. Appl Phys Lett, 2007, 91(12): 121103

[5] Chao C Y, Fung W, Guo L J, et al. Polymer microring resonators for biochemical sensing applications. IEEE J Sel Topics Quantum Electron, 2006, 12(1): 134

[6] De Vos K, Bartolozzi I, Schacht E, et al. Silicon-on-insulator microring resonator for sensitive and label-free biosensing. Opt Express, 2007, 15(12): 7610

[7] Saarinen J J, Weiss S M, Fauchet P M, et al. Optical sensor based on resonant porous silicon structures. Opt Express, 2005, 13(10): 3754

[8] Lin V S Y, Motesharei K, Motesharei K, et al. A porous silicon-based optical interferometric biosensor. Science, 1997, 278: 5339

[9] Block I D, Chan L L, Cunningham B T. Photonic crystal optical biosensor incorporating structured low-index porous dielectric. Sensors and Actuators B, 2006, 120(1): 187

[10] Chakravarty S, Topol'ancik J, Bhattacharya P, et al. Ion detection with photonic crystal microcavities. Opt Lett, 2005, 30(19): 2578

[11] Lee M, Fauchet P M. Two-dimensional silicon photonic crystal based biosensing platform for protein detection. Opt Express, 2007, 15(8): 4530

[12] Lee M R, Fauchet P M. Nanoscale microcavity sensor for single particle detection. Opt Lett, 2007, 32(22): 3284

[13] Yablonovitch E, Gmitter T J. Donor and acceptor modes in photonic band structure. Phys Rev Lett, 1991, 67(24): 3380

[14] Painter O, Vučovič J, Scherer A. Defect modes of a two-dimensional photonic crystal in an optically thin dielectric slab. JOSA B, 1999, 16(2): 275

[15] Kwon S H, Sünner T, Kamp M, et al. Optimization of photonic crystal cavity for chemical sensing. Opt Express, 2008, 16(16): 11709

[16] Vučović J, Lončar M, Mabuchi H, et al. Design of photonic crystal microcavities for cavity QED. Phys Rev E, 2001, 65(1): 1